

# A Fast DRR Generation Scheme for 3D-2D Image Registration Based on the Block Projection Method

Zhiping Mu

Perspective Pixel Technologies

16192 Coastal Highway, Lewes, DE 19958

mzp@ieee.org

## Abstract

*In three-dimensional to two-dimensional (3D-2D) image registration, DRR (digitally reconstructed radiograph) generation is often a bottleneck in computation. In this article, a novel fast DRR generation scheme is proposed based on the recently introduced Block Projection method and Slab algorithm that reuse building blocks of DRRs previously generated for known poses. The scheme is flexible as exemplified in pose grid design and slab binding, and upper bounds in projection error exist and can be estimated. Experiments were conducted to evaluate DRR quality and sensitivity to pose difference; computing time and error bounds were reported. The results showed that on a conventional computer the proposed scheme generated high quality, pose-preserving DRRs of size  $512 \times 512$  in 6 ms with slab binding, demonstrating its potential to be a viable solution to fast, high quality DRR generation for 3D-2D image registration.*

## 1. Introduction

Image guidance has become a daily practice in clinical institutions around the world; it provides unprecedented positioning accuracy and improves quality of treatment, vital to many clinical procedures such as biopsy [1,2], surgery [3], interventional procedures [4], and radiation treatments [5]. For example, in image-guided radiotherapy (IGRT), the pre-operative image is usually the 3D computed tomography (CT) image used for treatment planning. At treatment time, intra-operative images are acquired and compared with pre-operative images to determine alignment errors. Compared with 3D modalities such as Cone Beam CT, 2D X-ray imaging is often chosen for intra-operative imaging due to its fast acquisition and low imaging dose, and 3D-2D image registration is usually employed to register the 3D pre-operative CT image with 2D X-ray images acquired with patient on the treatment

couch [6].

Since 3D and 2D images cannot be directly registered, the 2D intra-operative images are usually registered with synthetic images called DRRs. DRRs are simulated X-ray like images created from a 3D CT image by placing the 3D volume (represented by that CT image) in specific poses within a virtual imaging system that simulates the actual X-ray imaging geometry.

Conventional registration algorithms usually operate iteratively: start with a hypothetical pose, create DRRs for that pose, evaluate similarity with intra-operative images, and search for the next potential pose; then generate DRRs for this new pose, and the iteration goes on. During the search step, DRRs may be generated for multiple poses close to the current pose for numerical estimation of derivatives. For example, if the algorithm employs a 6D search (i.e., 3D translation and 3D rotation), additional DRRs will be generated for six close poses just for a gradient estimation at one pose. Typically DRRs will be generated for hundreds of times during registration.

DRR generation is computationally intensive by nature. In general, there are two types of methods for DRR generation. The most commonly used algorithm is ray casting, where each pixel value is a line integral of the CT values of the voxels on the path of the beam incidental on that pixel, similar to image order volume rendering in computer graphics [7]. Another approach is similar to object order rendering [8], called voxel projection, treating DRR as a sum of all voxel projections [9]. Both methods bear a high complexity level of  $O(n^3)$ . In comparison, similarity measure computation is on the 2D images, and usually has a complexity level of  $O(n^2)$ .

Given its complexity and frequency of execution during registration, faster DRR generation methods are highly desired. For the voxel projection approach, if there are less voxels to render, less computation. It has been proposed to remove soft tissue voxels and calculate only bony tissue voxels. It was reported that a factor of 10-20 in time reduction had been achieved with this approach [10]. However, this method gains on speed at the cost of lost

soft tissue information, limiting the registration algorithm to rely solely on bony structures, and subsequently limiting its application in regions with primarily soft tissue organs such as liver and lung. And there is little room for further improvement on time reduction.

Another approach to achieve time reduction is to trade space for time, storing off-line pre-generated results for quick on-line computation. Methods such as light field and progressive attenuation field have been proposed to compute DRR using previously generated rays [7][11][12]. For example, in the light field method, each ray is computed by interpolation of several rays of similar poses [7][11]. Theoretically, the light field method requires a dense sampling of the 4D ray space for high DRR quality, and reduces the complexity level from  $O(n^3)$  to  $O(n^2)$ , and substantial time reduction has been reported [7].

It is worth to note that in the light field method, because a new ray is approximated using whole rays, it inevitably involves voxels that are not on the path of the new ray, as shown in Fig. 1A, resulting in errors that are difficult to estimate or control.

A new fast DRR generation method, the Block Projection method, and its sample implementation, the Slab algorithm, have been introduced recently based on the idea of ray segment approximation [13]. As shown in Fig. 1B, if a new ray is approximated by ray segments close to its path, contribution from external voxels can be substantially suppressed. In this method, a 3D volume is divided into blocks; block projections are pre-generated for a number of known poses, and new DRRs are created by re-projecting and assembling these block projections. In essence, it reuses ray segments instead of whole rays (note that each pixel in the block projection represents a ray segment). Because there are a much smaller number of blocks to process at runtime, DRRs can be computed for

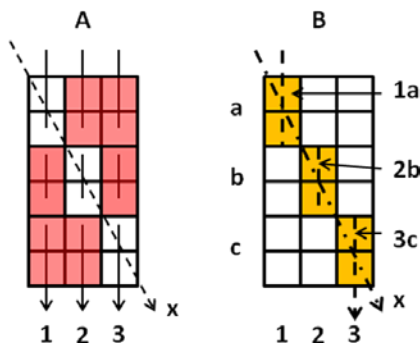


Fig. 1 Illustration of whole ray approximation and ray segment approximation. A. Whole ray approximation. If a new ray  $x$  is calculated by interpolation of existing rays 1-3, the boxes in red are not on the path of  $x$  but will contribute to  $x$ . B. Ray segment approximation. If the rays are divided into segments, the new ray  $x$  may be better approximated by ray segments 1a-2b-3c.

new poses at high efficiency. The results showed that this method significantly reduced computing time for online DRR generation while maintained very high quality [13].

Parallel to the algorithmic improvements, acceleration through implementation on GPUs [14][15] has gained a lot of attention recently, and computing time in a few milliseconds and speed-up ratio up to 98 times of an equivalent CPU-based approach have been reported [15].

In this article, a fast DRR generation scheme based on the Block Projection method is proposed for 3D-2D image registration, and results are presented to validate the proposed scheme and slab binding approach.

## 2. Method

In this section, a brief introduction of the Block Projection method and the Slab algorithm [13] is given first. Then a fast DRR generation scheme suitable for 3D-2D registration is proposed, and important new elements of the scheme such as pose grid, projection error estimation and slab binding are discussed.

### 2.1. The Block Projection method

The structure of the Block Projection method is rather straightforward. It consists of an offline pre-processing part and an online DRR generation part, as shown in Fig. 2. Note that the block projection can be created with any existing method such as ray casting [7] or splatting [16], just treating each block as a separate volume. As an implementation of this method, the Slab algorithm was introduced in [13], and is listed below for readers' convenience.

#### Slab Algorithm

1. Pre-generation of slabs for a number of known poses
  - (a) For every known pose, compute projections of all slices
  - (b) Calculate the sum of every  $N$  consecutive slice projections as synthetic block projections,  $B_N$ , or slabs
2. To generate DRR for a new pose,
  - (a) identify the closest known pose and associated slabs,  $B_N$
  - (b) Re-project slabs,  $B_N$ , to compute their projections for a new pose,  $P_N$
  - (c) Sum  $P_N$  to obtain the new DRR

where  $N$  represents the slab thickness. For convenience, a Slab algorithm with a thickness of  $N$  slices is called an  $S(N)$  algorithm, and DRRs it generates are called "slab DRRs". Note that step 2(a), identifying the closest pose, need only to be calculated once for each DRR instead of for each ray as in the light field method. Hence time required for this step is negligible. It is also worth to note that the slices may be the native slices in CT, such as the coronal or sagittal slices, depending on the projection

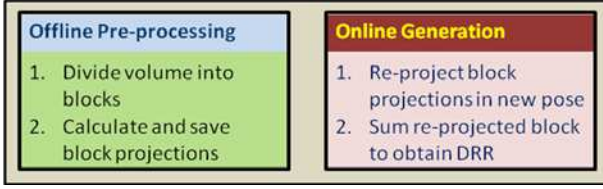


Fig. 2 Diagram of the Block Projection method.

angle. It works the best if the slices are perpendicular to the optical axis. And the algorithm may be extended so that the CT slices are projected to the imager plane one by one, interpolated to the pixel matrix, and summed to compute DRR [13]. This method is used in the next section to create slabs and “standard” DRRs.

The Block Projection method is flexible and polymorphic (borrowing the concept from object oriented programming). In addition to the “plug-and-playability” of any existing method for creating block projections, it may be implemented with different ways of volume partition suitable to the application. For example, in the Slab algorithm, the volume is divided into slices. Hence it would make a good choice in 2D imaging guidance where the anteroposterior (AP) and lateral views are usually taken, and the coronal and sagittal slabs may be created respectively.

## 2.2. Pose grid

An important component to customize is the configuration of poses to pre-generate slabs for, called “pose grid”, and a pose in the grid is called a “grid pose”. Take IGRT as an example. A patient is first manually aligned to treatment position based on in-room laser and body marks, and then image guidance is applied to find residual alignment errors, which are usually less than one centimeter in translation and a few degrees in rotation. Here image guidance does not need to operate in open space, but rather serves as a precise alignment tool in short range following a gross alignment. In addition, it is reported in [13] that the algorithm is insensitive to rotations around the optical axis, maintaining high quality even at large slab thickness. Therefore, slabs may only need to be pre-generated for poses with rotations around the other two in-plane axes. Shown in Fig. 3 are two sample pose grids with nine and seven poses, respectively.

## 2.3. Projection error

An advantageous feature of the Block Projection method is the deterministic nature of voxel projection geometry. Voxel projection position error is a result of slab re-projection, and can be thereby estimated. As shown in Fig. 4, to compute the projection X using slabs created for

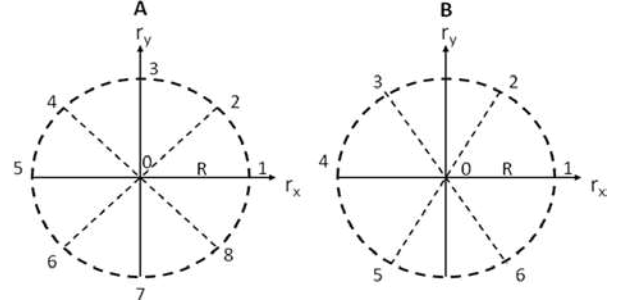


Fig. 3 Illustration of pose grid. A. Nine-pose grid. B. Seven-pose grid. The poses are evenly distributed on a circle in rotational space.  $r_x$ ,  $r_y$ : rotation around x and y axis, the in-plane axes. R: radius of the circle.

projection 1, according to the algorithm, the voxel in white is projected to the same position as the voxel in gray of the same slab that is at the center slice, resulting in an error  $d$  that is given by

$$d = D \sin(\alpha). \quad (1)$$

For the slabs with a thickness of  $N$  slices, and let the pixel size in the direction of projection 1 be  $p$ , then the maximum value for  $D$  is  $Np/2$ , and the maximum error,  $d_{\max}$ , would be

$$d_{\max} = Np \sin(\alpha)/2. \quad (2)$$

This represents the upper bound of projection error. For small angle differences, i.e., small  $\alpha$ s, it can be further simplified as

$$d_{\max} \approx Np\alpha/2, \quad (3)$$

where  $\alpha$  is in radians. Voxel projection position error in the Block Projection method in general can be extended

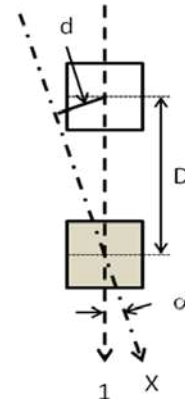


Fig. 4. Illustration of projection position error resulting from slab re-projection. The box in gray represents a voxel at the center slice of a slab. If slabs are created for projection 1, and a new projection X is to be computed, for a voxel (in white) in the same slab as the gray voxel, the position error in projection X would be  $d$ .  $D$  is the separation between the two voxels, and  $\alpha$  is the angle between projection 1 and X.

from this analysis. It can be used as a general guideline in selection of pose grid and slab thickness for a given maximum projection error. Note that translation induced pose difference can be converted to angle difference for projection error estimation.

## 2.4. Slab binding

As shown in Eq. (1-3), the position error depends on slab thickness and angle difference. To contain projection error, one may choose either to create slabs with small thickness or for more poses, both at the cost of memory space. Fortunately, the way the volume is partitioned and the slabs are stored allow for slab binding, i.e., multiple slabs can be added together to form thicker slabs before re-projection in the Slab algorithm. Slab binding is a simple pixel-to-pixel summation, and can be done in a relative small fraction of time in comparison with re-projection, which consists of mainly interpolations. This way slabs can be created for small thickness and bound at run time if the angle difference is small, at a minor cost of slab summation computation.

It is indicated earlier that most registration algorithms employ a search strategy to find the next potential pose, and derivatives are estimated numerically in the course. Slab binding is particularly useful in computation of derivatives, where DRRs are generated for poses slightly offset from the current pose. For this purpose, slab binding may be performed after the original slabs are re-projected for the current pose, and then the re-projected slabs can be bound for re-projection again for the offset poses. Note that slabs need to be bound only once when computing derivatives in multiple directions at one pose.

## 2.5. DRR generation scheme

Illustrated in Fig. 5 is a diagram of DRR generation scheme for 3D-2D image registration. Slab binding steps are optional depending on the pose differences. Note that runtime slabs are temporarily stored slabs re-projected from grid pose slabs that can be used for slab binding.

## 3. Results

A head phantom CT scan was used for experimentation, which was  $512 \times 512 \times 208$  in size with voxels in size of  $0.588 \times 0.588 \times 1.25 \text{ mm}^3$ . In the experiments, the original pose was the AP projection of the head phantom placed in its native orientation as captured in the CT scan. The X-, Y-, and Z- axes were defined as left-right, superior-inferior, and anterior-posterior directions of the head phantom.

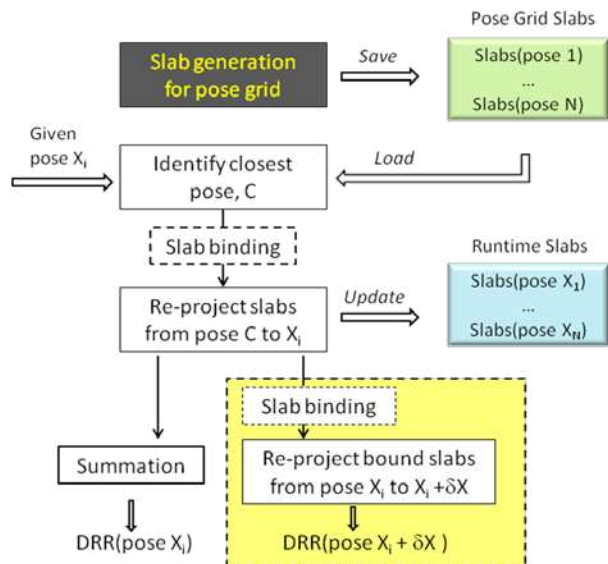


Fig. 5 Diagram of DRR generation based on the Slab algorithm. The operation in gray box represents offline processing, and online operations in white boxes. 3D boxes in green and blue are data used and updated during operation. Operations in the yellow rectangle are for derivative

As discussed above, the error in the proposed DRR generation scheme is mainly affected by two factors, the slab (or block) thickness and the pose difference, namely the angle difference. In order to achieve fast online DRR generation at desired accuracy, it is important to study how error is affected by slab thickness.

In the first experiment, standard DRR was created for the 9 test poses, i.e., with 2, 2.5, and 3 degree rotations around the three axes, respectively. Slabs of thicknesses varying from 5 to 40 slices were created for the original pose; then slab DRRs for the 9 test poses were created with the Slab algorithm using these slabs. Shown in Fig. 6 are the standard and S(40) slab DRRs for the test poses with 3 degree rotations around the three axes, the extreme cases (largest thickness with largest rotation) in this experiment. Even at a large slab thickness, the differences between standard and slab DRRs of the same pose were very small and visually difficult to tell, demonstrating the high quality of the slab DRRs. Note that the pixel values in difference images were multiplied by a factor 10 for visualization. As expected, the difference is more eminent near edges, and exhibits a somewhat directional pattern, horizontal for rotation around x-axis (first row) and vertical for y-axis (second row).

The peak signal-to-noise ratio (PSNR) was calculated as a measure of error on intensity, which is given by [7]

$$\text{PSNR} = 10 \log_{10}(s^2/e_{\text{mse}}), \quad (4)$$

where  $e_{\text{mse}}$  is the mean squared error between a standard DRR and a slab DRR of the same pose, and S is the

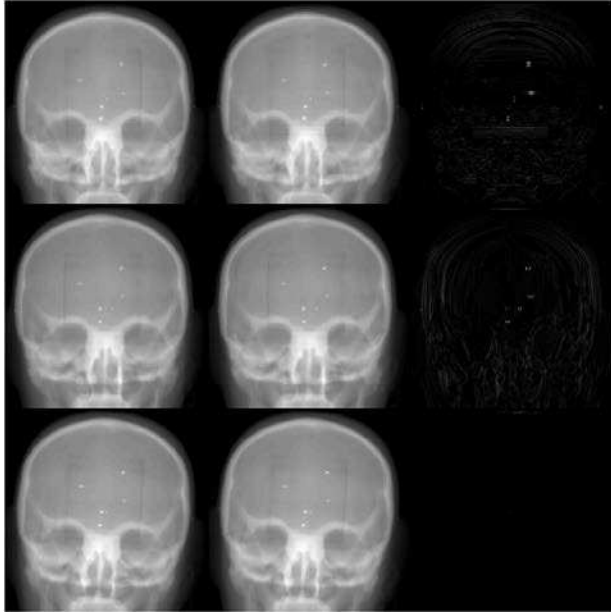


Fig. 6 Comparison of standard and slab DRRs. Left to right: standard DRRs, slab DRRs generated by S(40) algorithm, and their difference images; Top to bottom: generated for poses of 3 degree rotations around the X, Y, and Z axis, respectively. The pixel values in the differences were multiplied by a factor of 10 for better visualization.

maximum pixel value in the image.

Drawn in Fig. 7 are PSNR values of slab DRRs generated for 2, 2.5, and 3 degrees using slabs of different thicknesses. As shown in Fig. 7, the PSNRs in general decrease as N and angle increase, but remain greater than 50 dB for 2 and 2.5 degrees, and greater than 47 dB when N=40 at 3 degree. This result is encouraging because it demonstrates the algorithm generates DRRs of high quality

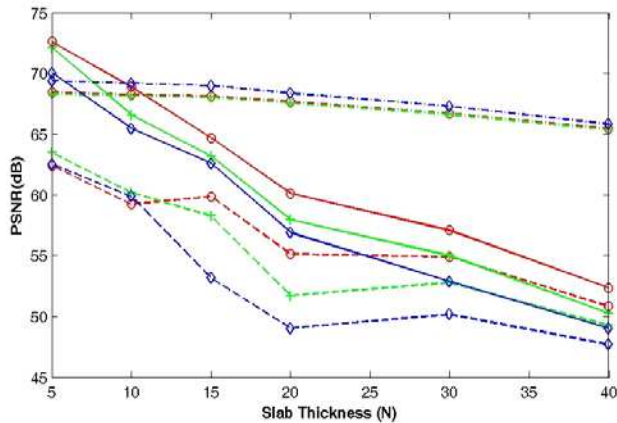


Fig. 7 Values of PSNR of slab DRRs generated for poses with 2 (red circle), 2.5 (green +), and 3 (blue diamond) degree rotations around X (solid), Y (dash) and Z (dash dot) axes using the Slab algorithm with different thickness, N.

with much higher efficiency. In comparison, the PSNR plateaued below 50 dB with the light field method [3]. It is worth mentioning that the PSNRs decrease less than 5 dB as N increases from 5 to 40, and remain above 65 dB for up to 3 degree rotation around the Z-axis (dash-dot lines in Fig. 7), which is parallel to the optical axis. This result is consistent with the preliminary results reported in [13] and helpful in designing the pose grid for slab generation.

DRRs are generated for image registration, and the goal of registration is to find the pose difference between the images. Therefore, in addition to pixel-to-pixel intensity accuracy measured by PSNR, it is critical to evaluate whether the DRRs faithfully capture the poses they are created for. In the next experiment, standard DRRs were generated with rotations of 2 and 3 degrees around the three axes. Slab DRRs were generated with S(20) and S(40) algorithm for poses with rotations of -2 to 6 degrees (at 1 degree step) around the three axes, respectively, using slabs created from the original pose (i.e., no rotations). Then mutual information (MI), as a similarity measure, was calculated between the standard DRRs and their corresponding slab DRRs (i.e., in poses with rotations around the same axes). Here MI between two image  $I_1$  and  $I_2$  is given by

$$MI(I_1, I_2) = H(I_1) + H(I_2) - H(I_1, I_2), \quad (5)$$

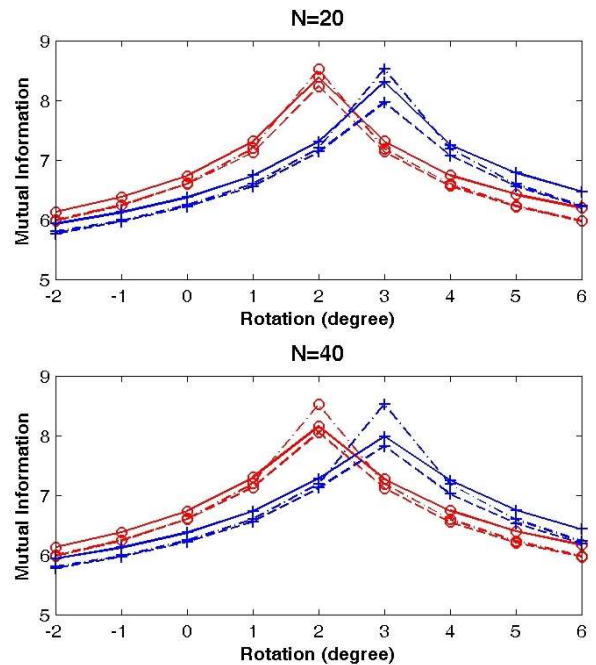


Fig. 8 Mutual information between standard DRRs of 2 (red circle) and 3 (blue +) degree rotations and slab DRRs created for different rotations around the same axes. Solid, dash, and dash dot lines are for rotations around X, Y, and Z axes. N is the slab thickness.

where  $H(I_1)$  and  $H(I_2)$  are entropies of the two images, and  $H(I_1, I_2)$  is the joint entropy of the two images. The results are plotted in Fig. 8. As shown, the curves have peaks at 2 and 3 degrees, which means the best matches by mutual information are found between DRRs of the same pose, and the values decrease sharply as the pose differences (rotation) grow bigger. These results suggest that the DRRs generated by the Slab algorithm preserve subtle pose-differentiating information vital to image registration, even at large slab thickness such as  $N=40$  used in this experiment.

It has been suggested in section 2 that a very large slab thickness ( $>40$ ) may be used to evaluate for poses with very small difference, such as in derivative or gradient computation when searching for the next potential pose. For example, suppose the initial hypothetical pose is the original pose, which is usually the case. To estimate gradient numerically, a small step size of 0.2 degree may be used, and one will need to generate DRRs for 0.2 degree rotations around the three axes. To evaluate the DRR quality in the large slab thickness, small angle case, slab DRRs with thickness varying from 20 to 120 were generated using the slabs created from the original pose. Note that results for slab thickness greater than 40 were obtained through slab binding using slabs of thickness 20. The PSNR values are plotted in Fig. 9. In general, they exhibit similar trend as the ones in Fig. 7, i.e., PSNR decreases as the thickness increases for rotation around the X and Y axes, but not affected much for rotation around the Z axis, which is the optical axis of projection in this case. And even at extremely large thickness of 120 slices, the PSNR is still greater than 58 dB for all three curves, demonstrating the high quality of slab DRRs and validating the idea of using large thickness for derivative estimations.

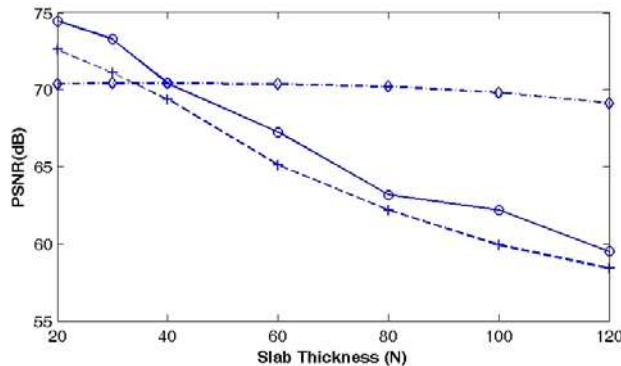


Fig.9. Values of PSNR of slab DRRs generated for poses with 0.2 degree rotations around X (solid), Y (dash) and Z (dash dot) axes using Slab algorithm with different thickness, N

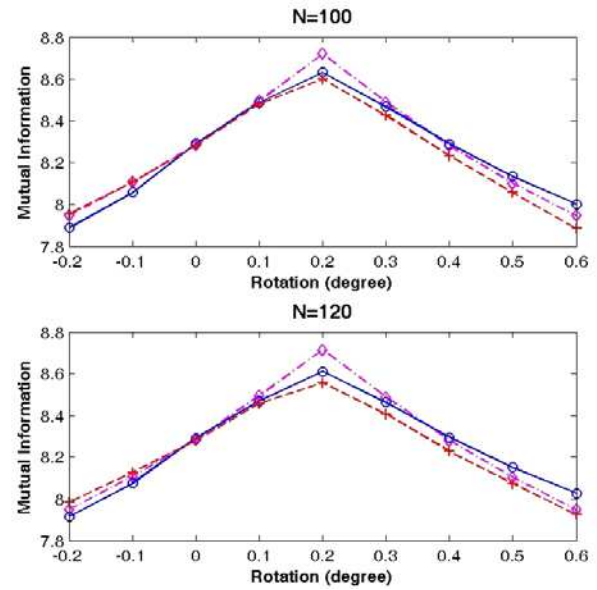


Fig.10. Values of mutual information between standard DRRs of 0.2 degree rotations and slab DRRs created for different rotations around the same axes. Solid, dash, and dash dot lines are for rotations around X, Y, and Z axes. N is the slab thickness.

To further evaluate whether the slab DRRs created with such large slab thicknesses preserve the critical pose information, now very subtle given the small pose difference of 0.2 degree, MI was calculated and plotted in Fig. 10. The curves all have peaks at 0.2 degree, illustrating that even when very large slab thicknesses such as 100 and 120 slices were used, the slab DRRs still preserved the critical pose information to correctly identify the very small angle of rotation, exemplifying its feasibility for fast and accurate numerical derivative estimation during registration.

It was reported in [13] that the slab algorithm achieved a reduction in execution time by a factor of 60, generating a S(40) slab DRR in 62 ms compared with 3.8 seconds for a standard DRR on a computer equipped with an Intel Core2 Duo CPU. In this study, more extensive tests were conducted on a more advanced computer equipped with an Intel Core i7 3.4 GHz CPU and 8 GB memory, and the focus was on the performance of slab binding.

As a baseline, execution time to generate slab DRRs of size  $512 \times 512$  with S(10), S(20), S(30), and S(40) algorithms were recorded at 80, 40, 23, and 18 ms. Base slabs of thickness 10, 20, and 40 were used for slab binding to reach large thickness before re-projection, and the execution times are listed in Table 1.

Table 1. Execution time (in ms) with slab binding. Base X indicates that slabs of thickness X were used to bind multiple times to reach thickness indicated in the top row.

Thickness	40	60	80	100	120
Base 10	26	20	14	N/A	N/A
Base 20	19	17	14	12	10
Base 40	18	N/A	10	N/A	6

The maximum voxel projection position errors for thicknesses and angle differences used in this section were calculated using Eq. (2). The results are listed in Table 2. As shown, projection error bounds are smaller than 0.5 mm for thickness up to 30 with angle difference up to 3° (shaded cells). And at small angle difference (0.2°), projection error is only around 0.1 mm even at very large slab thickness (100 or 120), validating the strategy to generate DRR for derivative estimation with large slab thickness through slab binding.

Table 2. Maximum voxel projection position errors (in mm) for different slab thickness and angle difference. Shown in shaded cells are values less than 0.5 mm. CT pixel size, p, is 0.588mm.

N	0.2°	1.0°	2.0°	2.5°	3.0°
10	0.0103	0.0513	0.1026	0.1282	0.1539
20	0.0205	0.1026	0.2052	0.2565	0.3077
30	0.0308	0.1539	0.3078	0.3847	0.4616
40	0.0411	0.2052	0.4104	0.5130	0.6155
60	0.0616	0.3079	0.6156	0.7694	0.9232
80	0.0821	0.4105	0.8208	1.0259	1.2309
100	0.1026	0.5131	1.0260	1.2824	1.5387
120	0.1232	0.6157	1.2313	1.5389	1.8464

#### 4. Discussions

As mentioned above and verified by the results, in the proposed DRR generation scheme, computing time is affected mainly by slab thickness, N. Since there is n/N slabs (each with roughly  $n^2$  elements) to re-project at run time, the computational complexity is  $O(n^3/N)$ . Given the common parameters of  $n \leq 512$ , and N varies from 10 to over 100, the complexity is effectively on the same order as  $O(n^2 \log(n))$ .

A key element of the proposed DRR generation scheme is the pose grid to pre-generate slabs for, which affects both speed and accuracy. An obvious option is a cube or sphere in the 3D rotational space. As suggested in section 2 and verified by the results in section 3, DRR quality is not affected much by slab thickness if the pose difference is for rotation around the optical axis (Fig. 7 and 9). Therefore, the pose grid may be further simplified, consisting of only rotations around the two in-plane axes,

evenly distributed on a circle in the  $r_x$ - $r_y$  space as illustrated in Fig. 3.

One may design pose grid based on application, and choose slab thickness according to desired accuracy. For example, if the radius, R is chosen to be 5° for a nine-pose grid, for a vast majority of poses with differences less than 7.5°, there exists a grid pose within 2.5°. And results in the previous section show that high quality DRRs may be obtained even with large slab thickness for such a small pose difference. This pose grid may be a good choice for application such as IGRT where the residual alignment error is small, usually within a few degrees from planned position. Translation induced pose difference is usually less than 2 degrees because the source-to-object distance, represented as SAD (source-axis distance) or SSD (source-surface distance), in the imaging system is much larger than translation. Slab thickness between 20 and 40 may be chosen so that the slab DRRs have high quality (PSNR > 50 dB as shown in Fig. 7), and the maximum projection errors are less than the pixel size in CT (Table 2). If slab thickness of 20 is chosen, there would be at most 26 slabs for each pose, and a total of 234 slabs for 9 poses; the slabs are about the same size as the DRR which is 512×512 in this study; the slabs are stored in floating point numbers, hence the total size of the slabs in this case is about 234 MB, similar to one or two CT dataset, and can be accommodated with ease by conventional computers. Choice of larger thickness would reduce the size of grid slabs and increase DRR generation speed, but at the cost of decreased accuracy.

Slab binding offers additional flexibility in handling the trade-off among speed, space, and accuracy, and can be employed based on the projection error bound given by Eq. (2). For example, during registration, if a new potential pose Y is only 1° away from a grid pose G, then base 20 slabs for pose G can be bound 2 to 4 times to generate DRR for pose Y, depending on the desired accuracy. And as suggested in section 2 and verified by results in section 3, slab binding can always be employed in generating DRRs for derivative estimation. Therefore, in a registration algorithm utilizing a 6D search, at a given pose, typically one DRR is generated for similarity evaluation and at least 6 DRRs are generated for gradient estimation. Taking computing times from table 1, an S(20) DRR for similarity evaluation takes 40 ms, and 6 DRRs for gradient estimation takes 6 ms each (base 20, bound 6 times for N=120), it would total at 76 ms. If two orthogonal views are taken for image guidance, then full resolution DRRs generation at each iteration would take 152 ms. Note that opportunities exist for further reduction when getting close to a grid pose, or operating at lower resolution if a multi-resolution approach is taken in the registration algorithm. Typically full resolution DRRs are only needed at later stage of the iterations.

The proposed DRR generation scheme is flexible and efficient, demonstrating great potential to be used for 3D-2D image registration. Despite the encouraging results, the proposed method is a framework still at early stage of development, and more rigorous testing and further investigations are warranted in the future. Experiments with more datasets from different body parts and performance incorporated in registration are needed to further evaluate its performance. For example, as shown in Fig. 6, the difference between standard and slab DRRs are mainly from bony structures. Hence segmentation of soft tissue and bony anatomy may be incorporated in the scheme, creating slabs separately with different thickness, smaller thickness for bony anatomy and larger for soft tissue. In addition, because 3D anatomic information is partially preserved in the slabs structure, it allows 3D deformation during registration, because the slabs can be manipulated individually prior to re-projection. Furthermore, this novel method is highly parallel in nature and suitable for deployment on GPUs, and CUDA implementation is currently under investigation. Considering the typical speed-up factors by GPU over equivalent CPU-based implementation were reported to be greater than 50 except for small CT datasets [15], the computing time may be further reduced to sub-millisecond level, making real time or near real time registration possible.

## 5. Conclusion

In this study, a fast DRR generation scheme is proposed based on the Block Projection method, where ray segments are pre-generated and reused. It offers flexibility and efficiency in pose grid design and slab binding. An important advantage is the existence of an upper bound for projection error thanks to the deterministic nature of the projection geometry of each voxel. Therefore appropriate parameters can be selected based on the application's requirement. The results presented in this article demonstrate that DRRs can be generated efficiently at high quality and with small projection error, suitable for 3D-2D image registration. In particular, a  $512 \times 512$  DRR generated for derivative estimations, which represents a large portion of all DRRs generated during registration, can be computed in 6 ms on a conventional Intel i7 computer, with PSNR greater than 58 dB and correctly identifying the small pose difference. And there is room for further time reduction with hardware acceleration.

## References

[1] A. V. D'amico, C. M. Tempany, R. Cormack, N. Hata, M. Jinzaki, K. Tuncali, M. Weinstein, and J. P. Richie. "Transperineal magnetic resonance image guided prostate

biopsy." *The Journal of urology*, Vol. 164, no. 2 (2000): 385-387.

[2] R.M. Pijnappel, M. Van den Donk, R. Holland, WP Th M. Mali, J. L. Peterse, J. H. C. L. Hendriks, and P. H. M. Peeters. "Diagnostic accuracy for different strategies of image-guided breast intervention in cases of nonpalpable breast lesions." *British Journal of Cancer*, Vol. 90, no. 3 (2004): 595-600.

[3] W. Grimson, L. Eric, J.Gil, S. J. Ettinger, T. Lozano-Perez, W. M. Wells, R. Kikinis. "An automatic registration method for frameless stereotaxy, image guided surgery, and enhanced reality visualization." *Medical Imaging, IEEE Transactions on*, 15, no. 2 (1996): 129-140.

[4] Papademetris, Xenophon, Kenneth P. Vives, Marcello DiStasio, Lawrence H. Staib, Markus Neff, Sven Flossman, Nils Frielinghaus et al. "Development of a research interface for image guided intervention: Initial application to epilepsy neurosurgery." In *Biomedical Imaging: Nano to Macro, 2006. 3rd IEEE International Symposium on*, pp. 490-493. IEEE, 2006.

[5] D.J. Moseley, E.A. White, K.L. Wiltshire, T. Rosewall, M.B. Sharpe, J.H. Siewerdsen, J.P. Bissonnette, M. Gospodarowicz, P. Warde, C.N. Catton, and D.A. Jaffray. "Comparison of localization performance with implanted fiducial markers and cone-beam computed tomography for on-line image-guided radiotherapy of the prostate," *International Journal of Radiation Oncology\* Biology\* Physics*, 67(3), pp.942-953, 2007.

[6] J.Y. Jin, S. Ryu, K. Faber, T. Mikkelsen, Q. Chen, S. Li, and B. Movsas, "2D/3D image fusion for accurate target localization and evaluation of a mask based stereotactic system in fractionated stereotactic radiotherapy of cranial lesions", *Medical Physics*, vol. 33, no. 12, pp. 4557-4566, 2006.

[7] D.B. Russakoff, T. Rohlfing, D. Rueckert, R. Shahidi, D. Kim, C.R. Maurer Jr, "Fast calculation of digitally reconstructed radiographs using light fields", in *Proc. SPIE Medical Imaging 2003*, pp. 684-695, SPIE, 2003.

[8] P. Lacroute, M. Levoy, "Fast volume rendering using a shear-warp factorization of the viewing transformation", in *SIGGRAPH 94*, pp. 451-458, ACM, 1994.

[9] W. Birkfellner, R. Seemann, M. Figl, J. Hummel, C. Ede, P. Homolka, H. Bergmann, "Fast DRR generation for 2D/3D registration", in Duncan, J., Gerig, G., (eds.) *MICCAI 2005, LNCS* vol. 3750, pp. 960-967. Springer Berlin Heidelberg, 2005.

[10] W. Birkfellner, R. Seemann, M. Figl, J. Hummel, C. Ede, P. Homolka, H. Bergmann, "Wobbled splatting—A fast perspective volume rendering method for simulation of x-ray images from CT", *Phys. Med. Biol.*, vol. 50, no. 9, pp. N73-N84, 2005.

[11] D.B. Russakoff, T. Rohlfing, K. Mori, D. Rueckert, A. Ho, J.R. Adler Jr, and C.R. Maurer Jr, "Fast generation of digitally reconstructed radiographs using attenuation fields with application to 2D-3D image registration", *Medical Imaging, IEEE Transactions on*, vol. 24, no.11, pp.1441-1454, 2005.

[12] T. Rohlfing, D.B. Russakoff, J. Denzler, K. Mori, C.R. Maurer Jr, "Progressive attenuation fields: fast 2D-3D

- image registration without precomputation”, *Medical Physics*, vol. 32, no. 9, pp. 2870-2880 2005.
- [13] Z. Mu, “A Novel Fast DRR Generation Method by Reassembling Previously Generated Projection Blocks,” *2016 IEEE Intl. Conf. Biomed. Health Informatics*, Las Vegas, 2016
- [14] G.J. Tornai, G. Cserey, I. Pappas, “Fast DRR generation for 2D to 3D registration on GPUs”, *Medical Physics*, vol. 39, no. 8 , pp. 4795-4799, 2012.
- [15] O.M. Dorgham, S.D. Laycock, M.H. Fisher, “GPU accelerated generation of digitally reconstructed radiographs for 2-D/3-D image registration”, *IEEE Trans. Biomedical Engineering*, vol. 59, no. 9, pp. 2594-2603, 2012.
- [16] W. Birkfellner, R. Seemann, M. Figl, J. Hummel, C. Ede, P. Homolka, X. Yang, P. Niederer, and H. Bergmann, “Wobbled splatting—a fast perspective volume rendering method for simulation of x-ray images from CT”.*Physics in medicine and biology*, vol. 50, no. 9, p.N73., 2005